JCTC Journal of Chemical Theory and Computation

Article

pubs.acs.org/JCTC

A Site Density Functional Theory for Water: Application to Solvation of Amino Acid Side Chains

Yu Liu,[†] Shuangliang Zhao,*[,‡] and Jianzhong Wu*[,†]

[†]Departments of Chemical and Environmental Engineering and Mathematics, University of California, Riverside, California 92521, United States

[‡]State Key Laboratory of Chemical Engineering, East China University of Science and Technology, Shanghai, 200238, P. R. China

Supporting Information

ABSTRACT: We report a site density functional theory (SDFT) based on the conventional atomistic models of water and the universality *ansatz* of the bridge functional. The excess Helmholtz energy functional is formulated in terms of a quadratic expansion with respect to the local density deviation from that of a uniform system and a universal functional for all higher-order terms approximated by that of a reference hard-sphere system. With the atomistic pair direct correlation functions of the uniform system calculated from MD simulation and an analytical expression for the bridge functional from the modified fundamental measure theory, the SDFT can be used to predict the structure and thermodynamic properties of water under inhomogeneous conditions with a computational cost negligible in comparison to that of brute-force simulations. The numerical performance of the SDFT has been demonstrated with the predictions of the solvation free energies of 15 molecular analogs of amino acid side chains in water represented by SPC/E, SPC, and TIP3P models. For theTIP3P model, a comparison of the theoretical predictions with MD simulation and experimental data shows agreement within 0.64 and 1.09 kcal/mol on average, respectively.

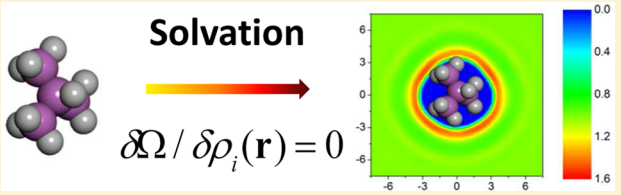

I. INTRODUCTION

In solution thermodynamics, solvation free energy (SFE) is typically defined as the reversible work to transfer a solute from a vacuum to a pure solvent at a given temperature and pressure (or equivalently, temperature and the solvent chemical potential). The thermodynamic concept is important not only for predicting liquid solubility but also for understanding virtually all chemical and biochemical processes in an aqueous environment including molecular recognition and binding affinity.[1−5] Despite a long history of theoretical developments, accurate prediction of SFE in water remains a daunting challenge.[6−11]

From a theoretical perspective, computational methods to study solvation may be classified into three categories: molecular simulation,[12−14] phenomenological methods,[2,15,16] and liquid-state theories.[1,17,18] Molecular simulation of SFE is mostly based on thermodynamic integration[19,20] and free-energy perturbation[11] calculations. With the advent of modern computers and rapid developments for semiempirical force fields, such calculations have been very popular over the past few decades. In principle, molecular simulation is exact and capable of predicting both the local solvent structure and the solvation free energy quantitatively. From a practical point of view, however, calculation of SFE using molecular simulation methods is computationally demanding, in particular for studying the solvation of large biomacromolecules. To avoid extensive numerical work, one may follow phenomenological methods such as various modifications of the Born model[2,3,15,16] or the Langevin−Debye model.[21,22] Such methods ignore the inhomogeneous behavior of solvent molecules near the solute surface, and neglecting the microscopic details makes the phenomenological calculations computationally very efficient and thus convenient for many practical applications. Regrettably, the phenomenological methods are often not accurate in comparison with simulation results or experimental data. Besides, they involve empirical parameters valid only for a narrow range of conditions.[23]

To a certain degree, liquid-state theories represent a compromise between simulations and phenomenological methods. Over the past decades, both the integral-equation theories[6,17,24,25] and the classical density functional theories[26−29] have been evolved into robust computational tools for predicting diverse properties of homogeneous and inhomogeneous liquid-state systems. On the basis of the different descriptions of the solvent configuration, the integral-equation theories can be further classified into molecular Ornstein−Zernike (MOZ) theories[6,24,30] and Reference Interaction Site Models (RISM).[1,31−35] In both cases, atomistic models can be used to describe the solvent molecules. While MOZ is focused on the molecular−molecular correlation functions, RISM deals with the intra- and intermolecular pair correlations between atomic sites. Because the correlation between atomic sites can be described by a three-dimensional function while that between molecules involves much higher dimensionality, applications of RISM to solvation, pioneered by Chandler[31,36] and thereafter greatly extended by Hirata and others,[32,33,35] have attracted much more

Received: December 12, 2012
Published: March 12, 2013

   dx.doi.org/10.1021/ct3010936 | J. Chem. Theory Comput. 2013, 9, 1896−1908

attention. It has been shown that 3D-RISM,[33,35] a recent improvement of RISM for SFE calculations, yields satisfactory results for a large number of solutes in water. Nevertheless, MOZ may have its own merits. In general, the theoretical framework behind RISM (including 3D-RISM) contains less information in comparison to that for the MOZ equation. In other words, the pair correlation functions of the RISM equation are insufficient to reproduce all multibody correlation effects described by the MOZ equation.[17]

In parallel to the integral-equation theories, both site and molecular descriptions of solvent molecules can be used as a basis to formulate the molecular density functional theories (MDFT). With the molecular direct correlation function of the bulk solvent obtained from the MOZ equation, Borgis and co-workers showed[26−29,37] that the solvation free energy can be calculated from the "homogeneous reference fluids approximation (HRFA);" namely, the unknown excess term is approximated by the angular-dependent direct correlation function of the pure solvent. A minimization of the solvation free energy (functional) with respect to the local molecular density profile leads to both the structural and energetic properties of the solvent system with an arbitrary solute. It has been shown that this approach is accurate for polar solvents such as acetonitrile. But for water, an empirical three-body correlation term must be incorporated in order to restore an accurate prediction of the hydration structure and free energies.[29] It has been pointed out that HRFA is equivalent to the hypernetted-chain (HNC) approximation in molecular integral theories.[29] Both theories can be obtained by the second-order truncation of the functional expansion of the excess Helmholtz energy with respect to that of a homogeneous system. We showed in a previous work[38] that the solvation free energy predicted through the molecular density functional theory with the density profile obtained from MD simulation can be further improved by complementing the higher-order terms with a reference hard-sphere bridge functional. Such a bridge functional can be incorporated into the minimization procedure to avoid the simulation input. Recently, Levesque et al. demonstrated that the predicted solvation free energy is more accurate than that from the HRFA approximation.[37]

The molecular density functional theory (MDFT) of solvation proposed by Borgis et al.[27,28,39] offers an excellent platform to study various properties of inhomogeneous molecular liquids. One caveat is that this approach is applicable only to systems with rigid molecules. Besides, a multidimensional description of the molecular positions and orientations requires quite large computational memory, and such demand together with the complexity of six-dimensional functional minimization hampers its many practical potentials. As proposed by Chandler, McCoy, and Singer (CMS),[40] the molecular density functional theory can be alternatively formulated in terms of the atomic density profiles. Unlike MDFT, the CMS theory is capable of treating both rigid and chain-like molecular fluids.[41−43] Because the CMS theory does not involve angular variables, it is simpler to implement and computationally more efficient in comparison with the high-dimensional approach.

In this work, we propose a new formulism for the prediction of solvation free energy following the site description of molecular densities and pair correlation functions. Although the current method is applicable to arbitrary molecular fluids, to avoid overlap with the existing MDFT,[29] we refer to our approach as three-dimensional Site DFT (SDFT) in contrast to the one-dimensional site-based density functional theory.[44] In essence, it is an extension of the CMS theory by incorporating the universality hypothesis of the bridge functional that was originally proposed by Rosenfeld[45] to account for the higher-order terms in the free-energy functionals of simple fluids. Different from conventional implementation of the CMS theory, however, we calculate the site−site direct correlation functions of the bulk reference system using MD simulation instead of the RISM equation. With the bridge functional represented by a reference hard-sphere system, the new formulism allows us to predict the solvation structure and the solvation free energy near quantitatively. While incorporation of the bridge functional greatly improves the numerical performance, the computational cost of the new formulism is comparable to that for the CMS theory.

To validate the numerical performance of the 3D-SDFT, we consider the solvation of 15 molecular analogs of amino acid side chains in water. These systems are selected as a benchmark of comparison because many computational works have been devoted to studying amino acid solvation.[5,7,13,14,46] Because the vapor pressures of amino acids are very low (typically 10^{14} times lower than that for water),[5,47] for direct comparison with experimental results, the computational studies are mostly focused on the SFEs of the neutral side-chain analogs.[13,19,48−50] For comparison with the simulation results, we follow a careful simulation work reported by Shirts and Pande.[13] In this work, 15 amino acid side chains were simulated with the OPLS-AA force field and six different classical models for water, i.e., SPC, SPC/E, TIP3P, TIP4P, TIP3P-MOD, and TIP4P-Ew. The first three models were used in this work for comparison. The SFE results were generated using the thermodynamic integration method through the usage of a large number of computers distributed around the world (via the folding@home program).[19] The solvation of amino acids has also been examined with different force fields as well as different simulation methods.[7,48−50] Notwithstanding the widespread usage, simulation of SFE is time-consuming. For each side chain, it may take up to thousands of CPU hours.[19] By contrast, the 3D-SDFT calculation can be done within tens of minutes.

The remainder of this article is organized as follows: In next section, we introduce the theoretical framework for the 3D-SDFT and its application to predicting solvation free energies in water. In section III, we present the numerical details for computation of the solvation structure and the solvation free energy for three different water models. Section IV gives the numerical results and discussions. Finally, we conclude in section V with a brief summary of this work and some prospects for future developments.

II. SITE DENSITY FUNCTIONAL THEORY FOR SOLVATION

The local solvent structure and the solvation free energy are two thermodynamic properties of central interest in studying solvation phenomena. In the following, we introduce the basic concepts and theoretical approximations in the site density functional theory that will be employed to predict both properties.

A. Solvent Density Profile. Consider a rigid solute of arbitrary geometry dissolved in a solvent at a given temperature and chemical potential. Let M be the number of atomic sites for the solute with their positions located at $\{\mathbf{r}_i\}$, $i = 1...M$. The density profiles of the solvent atoms (sites) near the solute are equivalent to those of an inhomogeneous system of the pure solvent in the presence of an external potential due to the solute−solvent interactions. Each solute site i exerts a potential on the

solvent molecules. The total external potential for each solvent site, $V_i^{\text{ext}}(\mathbf{r})$, is given by a summation of all solute sites, i.e.,

$$V_i^{\text{ext}}(\mathbf{r}) = \sum_{j=1}^{M} v_{ij}(|\mathbf{r} - \mathbf{r}_j|) \tag{1}$$

where $v_{ij}(|\mathbf{r} - \mathbf{r}_j|)$ is the potential between a solvent site at $\mathbf{r}$ and a solute site at $\mathbf{r}_j$. Following the CMS theory,[40] we express the grand potential in terms of the local densities of the solvent interacting sites:

$$\Omega[\rho_i(\mathbf{r})] = F^{\text{id}}[\rho_i(\mathbf{r})] + F^{\text{ex}}[\rho_i(\mathbf{r})] - \sum_i \int [\mu_i - V_i^{\text{ext}}(\mathbf{r})]\rho_i(\mathbf{r})\, \mathrm{d}\mathbf{r} \tag{2}$$

where $\rho_i(\mathbf{r})$ stands for the local density of solvent site i. In eq 2, F^{id} and F^{ex} represent the ideal and the excess contributions to the Helmholtz energy functional, respectively. The last term on the right side of eq 2 is directly related to the solute−solvent interactions. Different from that for a monatomic fluid, μ_i represents the nominal chemical potential of site i. The site chemical potentials from the same solvent molecule satisfies

$$\sum_i^{v} \mu_i = \mu_m \tag{3}$$

where v is the total number of sites for each solvent molecule, and μ_m is the solvent chemical potential. The ideal Helmholtz energy functional corresponds to that of an ideal solvent system with the same local density distribution but devoid of intermolecular interactions. Whereas this term can be written as a functional of the molecular density profile in a closed form, the ideal Helmholtz energy functional cannot be expressed only in terms of the site density profiles. Fortunately, as discussed later, such an expression is not necessary for SFE calculations. The excess free energy functional accounts for the effects of intermolecular forces and correlation effects; it is not dependent on the solute−solvent interactions explicitly.

As in our earlier work,[38] the excess free energy functional can be formulated relative to that of a uniform solvent at the same temperature and the solvent chemical potential:

$$F^{\text{ex}}[\rho_i(\mathbf{r})] = F^{\text{ex}}[\rho_i^b] + \sum_i \mu_i^{\text{ex}} \int \Delta\rho_i(\mathbf{r})\, \mathrm{d}\mathbf{r} - \frac{k_B T}{2} \sum_{i,j} \iint c_{ij}^{(2)}(|\mathbf{r} - \mathbf{r}'|)\Delta\rho_i(\mathbf{r})\, \mathrm{d}\mathbf{r}\, \mathrm{d}\mathbf{r}' + F^{\text{B}}[\rho_i(\mathbf{r})] \tag{4}$$

where $\Delta\rho_i(\mathbf{r}) = \rho_i(\mathbf{r}) - \rho_i^b$, ρ_i^b represents the bulk density of site i, μ_i^{ex} is the excess chemical potential of site i in the bulk solvent, and $c_{ij}^{(2)}(r)$ is the direct correlation function (DCF) between site i and site j in the bulk system. The last term in eq 4, $F^{\text{B}}[\rho_i(\mathbf{r})]$, takes into account all higher-order terms in the functional expansion. Conventionally, this term is called the bridge functional, which is related to the bridge function used in the liquid-state theory, $B_i(\mathbf{r})$

$$B_i(\mathbf{r}) = \frac{\delta\beta F^{\text{B}}[\rho(\mathbf{r})]}{\delta\rho(\mathbf{r})} \tag{5}$$

As indicated above, the excess free energy functional is intrinsic to the properties of the solvent molecules; it is influenced by the external energy only through the change in the atomic density profiles.

At equilibrium, the solvent density profile can be derived from a functional derivative of the grand potential with respect to the one-body potential, $\psi_j(\mathbf{r}) \equiv V_i^{\text{ext}}(\mathbf{r}) - \mu_i$:

$$\rho_i(\mathbf{r}) = \frac{\delta\Omega}{\delta\psi_j(\mathbf{r})} \tag{6}$$

After some algebra similar to that for eq A4 in the paper by Seok and Oxtoby,[41] eq 6 results in an implicit equation for the site density profile

$$\rho_i(\mathbf{r}) = \rho_i^b S_i(\mathbf{r}) \exp[-\beta V_i^{\text{ext}}(\mathbf{r}) + \sum_j \int \Delta\rho_j(\mathbf{r}')c_{ij}^{(2)}(|\mathbf{r} - \mathbf{r}'|)\, \mathrm{d}\mathbf{r}' - B_i(\mathbf{r})] \tag{7}$$

where $\beta = 1/(k_B T)$, k_B is the Boltzmann constant, and T is the absolute temperature. As explained below, $S_i(\mathbf{r})$ represents the normalized intramolecular correlation function. For a simple fluid, $S_i(\mathbf{r}) = 1$, and eq 7 reduces to the conventional Euler−Lagrange equation.

For all water models considered in this work (SPC, SPC/E, and TIP3P), the normalized intramolecular correlation function is given by

$$S_\alpha(\mathbf{r}) = \frac{1}{8\pi^2} \int_{-1}^{1} \mathrm{d}\cos\theta \int_0^{2\pi} \mathrm{d}\phi \int_0^{2\pi} \mathrm{d}\phi' \exp[-\lambda_\beta(\mathbf{r}_\beta) - \lambda_\gamma(\mathbf{r}_\gamma)] \tag{8}$$

where α, β, and γ stand for three interaction sites from the same water molecule, i.e., one oxygen site and two hydrogen sites. In eq 8, $\lambda_i(\mathbf{r})$ is given by

$$\lambda_i(\mathbf{r}) = \beta V_i^{\text{ext}}(\mathbf{r}) - \sum_j \int \Delta\rho_j(\mathbf{r}')c_{ij}^{(2)}(|\mathbf{r} - \mathbf{r}'|)\, \mathrm{d}\mathbf{r}' + B_i(\mathbf{r}) \tag{9}$$

where $\mathbf{r}_\beta$ and $\mathbf{r}_\gamma$ represent the positions of the other two sites from the same water molecule, given the first site α located at $\mathbf{r}$.

Because of the asymmetry of oxygen and hydrogen sites in each water molecule, there are two sets of expressions for $\mathbf{r}_\beta$ and $\mathbf{r}_\gamma$. When α is referred to the oxygen site, the relative positions of the two hydrogen sites from the same water molecule are given by

$$\begin{cases} \mathbf{r}_\beta \equiv \mathbf{r}_{H_1} = \mathbf{r} + d_{\text{OH}}(\sin\theta\cos\phi,\ \sin\theta\sin\phi,\ \cos\theta) \\ \mathbf{r}_\gamma \equiv \mathbf{r}_{H_1} = \mathbf{r} + d_{\text{OH}}\mathbf{M}_{\theta,\phi}(\sin\Theta\cos\phi',\ \sin\Theta\sin\phi',\ \cos\Theta)^{\text{T}} \end{cases} \tag{10}$$

where d_{OH} is the OH bond length and Θ is the angle for ∠HOH, (θ, ϕ) are the Euler angles of the first OH bond, and ϕ' is the rotation angle of the second OH bond around the first one. Superscript T denotes the transformation of the Euler rotation transfer matrix, $\mathbf{M}_{\theta,\phi}$, which is used to change the coordinates from one frame to another by rotating the Euler angles (θ, ϕ). Following the right-hand clock rule, we have[18]

$$\mathbf{M}_{\theta,\phi} = \begin{pmatrix} \cos\theta\cos\phi & -\sin\phi & \sin\theta\cos\phi \\ \cos\theta\sin\phi & \cos\phi & \sin\theta\sin\phi \\ -\sin\phi & 0 & \cos\theta \end{pmatrix} \tag{11}$$

Alternatively, if α is affiliated with a hydrogen site, we have

$$\begin{cases} \mathbf{r}_\beta \equiv \mathbf{r}_O = \mathbf{r} + d_{OH}(\sin\theta\cos\phi,\ \sin\theta \\ \qquad \sin\phi,\ \cos\theta) \\ \mathbf{r}_\gamma \equiv \mathbf{r}_{H_2} = \mathbf{r}_O \\ \qquad + d_{OH}\mathbf{M}_{\theta,\phi} \\ \qquad (\sin\Theta'\cos\phi',\ \sin\Theta'\sin\phi',\ \cos\Theta')^T \end{cases} \tag{12}$$

where $\Theta' = \pi - \Theta$.

Equations7−12 consist of the key equations for determining the density profile of water molecules around a rigid solute of arbitrary geometry. To solve these equations numerically, we need additional knowledge on the site−site DCFs of bulk water as well as the bridge functional. Under specific thermodynamic conditions, the DCFs of bulk water can be calculated from molecular dynamics simulation (the computational details are reported elsewhere).[51,52] Different from the DCF of a simple fluid, the asymptotic behavior of the site−site DCFs does not follow the MSA limit. Instead, at large separation, the site−site DCF approaches

$$c_{\alpha\beta}(r) = -\zeta\beta u_{\alpha\beta}{}^{qq} \text{ when } r \to \infty \tag{13}$$

where $u_{\alpha\beta}{}^{qq}(r) = q_\alpha q_\beta/(4\pi\varepsilon_0 r)$ is the Coulomb potential between two sites with charges q_α and q_β, and ε_0 is the vacuum permittivity. Parameter ζ depends on the molecular model as well as the thermodynamic state; an analytical expression has been derived for water-like molecules.[51] For the three water models considered in this work, $\zeta_{SPC/E} = 0.9609$, $\zeta_{SPC} = 0.9584$, and $\zeta_{TIP3P} = 0.9586$ at $P = 1$ atm and $T = 298$ K.

It has been well documented that the bridge functional is mainly affiliated with short-range repulsion and excluded volume effects.[53] According to the universality *ansatz* of the bridge functional proposed by Rosenfeld,[45] the bridge functional is insensitive to the precise form of the solute−solvent interactions and can be approximated by that of a hard-sphere reference system with the same atomic density profiles. The properties of the latter system can be faithfully described by the fundamental measure theory (FMT)[53,54] and its modifications.[55,56] Rosenfeld demonstrated that the universality *ansatz* works well for a wide variety of systems including simple fluids and plasma.[53,57] In an earlier work,[38] we showed that the hypothesis holds also for accounting the excluded volume effects in molecular systems.

The excluded volume of water molecules mainly arises from the oxygen atoms. As a result, the bridge functional can be approximated by that of a hard-sphere (HS) system with the density profile the same as that for the oxygen site

$$F^B[\rho_i(\mathbf{r})] \approx F^B_{HS}[\rho_O(\mathbf{r})] \tag{14}$$

This assumption corroborates with all conventional molecular models of water including the three considered in this work. Similar to our earlier work,[38] the bridge functional of the corresponding HS system is calculated from the modified fundamental measure theory (MFMT)[55]

$$F^B_{HS}[\rho_O(\mathbf{r})] = F^{ex}_{HS}[\rho_O(\mathbf{r})] - F^{ex}_{HS\text{-}b} - \mu^{ex}_{HS\text{-}b}\int \Delta\rho_O(\mathbf{r})\,d\mathbf{r} + \frac{1}{2}k_BT\iint c^{(2)}_{HS\text{-}b}(|\mathbf{r}-\mathbf{r}'|)\Delta\rho_O(\mathbf{r})\Delta\rho_O(\mathbf{r}')\,d\mathbf{r}\,d\mathbf{r}' \tag{15}$$

where $F^{ex}_{HS}[\rho_O(\mathbf{r})]$ is the excess free energy functional of an inhomogeneous HS system with the density profile identical to that for the oxygen site; $F^{ex}_{HS\text{-}b}$, $\mu^{ex}_{HS\text{-}b}$, and $c^{(2)}_{HS\text{-}b}(r)$ are, respectively, the excess free energy, the excess chemical potential, and the direct correlation function for the bulk HS system.

By substituting eqs 15 and 14 into eq 5, we arrive at

$$\begin{cases} B_O(\mathbf{r}) = \beta\mu^{ex}_{HS}(\mathbf{r}) - \beta\mu^{ex}_{HS\text{-}b} \\ \qquad + \int c^{(2)}_{HS\text{-}b}(|\mathbf{r}-\mathbf{r}'|)\Delta\rho_O(\mathbf{r}')\,d\mathbf{r}' \\ B_O(\mathbf{r}) = 0 \end{cases} \tag{16}$$

where $\mu^{ex}_{HS}(\mathbf{r})$ is the local excess chemical potential of the inhomogeneous HS reference system. In this work, $F^{ex}_{HS}[\rho_O(\mathbf{r})]$,$c^{(2)}_{HS\text{-}b}(r)$, and $\mu^{ex}_{HS}(\mathbf{r})$ are all calculated from MFMT,[55] while $F^{ex}_{HS\text{-}b}$ and $\mu^{ex}_{HS\text{-}b}$ are calculated from the Carnahan−Starling equation of state.[58] To perform such calculations, we may define the HS diameter of the reference system by using an experimental input for either the bulk chemical potential of pure water or the hydration free energy of one representative solute.[38] In this work, we fix the HS diameter from the solvation free energy of methane, which is the simplest side chain analog of amino acids. The effective HS diameters are 2.91, 2.96, and 2.86 Å for SPC/E, SPC, and TIP3P water models, respectively.

Before ending this subsection, we should re-emphasize that the 3D-SDFT presented above is quite different from earlier developments of classical DFT. Although the above derivation closely follows the CMS theory, the treatment for the excess part of the Helmholtz energy functional is very different. Instead of using the RISM equation for the bulk fluid and the quadratic functional expansion, here we adopt accurate bulk DCFs and a reference HS bridge functional. Because the free-energy is formulated in terms of site densities instead of the molecular density, the 3D-SDFT is also different from the previous versions of the molecular DFT, even when the same hard-sphere bridge functional was used. Those differences, together with the new computational procedure for SFE calculations introduced below, consist of the key novelty of the present work.

B. Solvation Free Energy. The solvation free energy can be expressed as the change in the grand potential of a solvent at a given temperature and chemical potential upon dissolution of a single solute molecule

$$F[\rho_i(\mathbf{r});\ \mu_m,\ V,\ T] = \Omega[\rho_i(\mathbf{r});\ \mu_m,\ V,\ T] - \Omega[\rho_i{}^b;\ \mu_m,\ V,\ T] \tag{17}$$

where V is the system volume, which should be sufficiently large such that the properties of water molecules remote from the solute are the same as those corresponding to the bulk water. With the help of eq 2 and eq 4, the solvation free energy can be deduced as

$$F[\rho_i(\mathbf{r})] = \Delta F^{\mathrm{id}}[\rho_i(\mathbf{r})] - \sum_i \int V_i^{\mathrm{ext}}(\mathbf{r})\rho_i(\mathbf{r})\,\mathrm{d}\mathbf{r} - \sum_i \mu_i^{\mathrm{id}} \int \Delta\rho_i(\mathbf{r}) - \frac{k_\mathrm{B}T}{2} \sum_{i,j} \iint c_{ij}^{(2)}(|\mathbf{r}-\mathbf{r}'|)\Delta\rho_i(\mathbf{r})\Delta\rho_j(\mathbf{r}')\,\mathrm{d}\mathbf{r}\,\mathrm{d}\mathbf{r}' + F^{\mathrm{B}}[\rho_i(\mathbf{r})] \quad (18)$$

To determine the noninteracting part of the solvation free energy, $\Delta F^{\mathrm{id}}[\rho_i(\mathbf{r})] \equiv F^{\mathrm{id}}[\rho_i(\mathbf{r})] - F^{\mathrm{id}}[\rho_i^b]$, we may consider an inhomogeneous ideal-gas system that has the site density profile $\{\rho_i(\mathbf{r})\}$, the same as that of the real system. Because of the lack of intermolecular interactions in the ideal system, however, the external potential, $V_i^{\mathrm{ext-IG}}(\mathbf{r})$, should be different from that of the real system. In other words, the local density profile in the ideal reference system should be understood as that generated by an imaginary solute. Similar to eq 18, the solvation free energy of such an imaginary solute in the reference ideal-gas system can be written as

$$F_{\mathrm{IG}} = \Delta F^{\mathrm{id}}[\rho_i(\mathbf{r})] - \sum_i \int V_i^{\mathrm{ext\text{-}IG}}(\mathbf{r})\rho_i(\mathbf{r})\,\mathrm{d}\mathbf{r} - \sum_i \mu_i^{\mathrm{id}} \int \Delta\rho_i(\mathbf{r}) \quad (19)$$

The last two terms of eq 18 vanish due to the lack of intermolecular interactions in an ideal-gas system.

The solvation free energy of any solute in an ideal gas, F_{IG}, can be calculated analytically (see Appendix A)

$$F_{\mathrm{IG}} = -\frac{k_\mathrm{B}T}{v} \sum_{i=1}^{v} \int \Delta\rho_i(\mathbf{r})\,\mathrm{d}\mathbf{r} = -\Delta N k_\mathrm{B}T \quad (20)$$

where ΔN is the change in the average number of solvent molecules upon introduction of the solute molecule. A combination of eqs 18, 19, and 20 gives

$$F[\rho_i(\mathbf{r})] = \Delta N k_\mathrm{B}T + \sum_i \int [V_i^{\mathrm{ext}}(\mathbf{r}) - V_{\mathrm{IG},i}^{\mathrm{ext}}(\mathbf{r})]\rho_i(\mathbf{r})\,\mathrm{d}\mathbf{r} - \frac{k_\mathrm{B}T}{2} \sum_{i,j} \iint c_{ij}^{(2)}(|\mathbf{r}-\mathbf{r}'|)\Delta\rho_i(\mathbf{r}')\,\mathrm{d}\mathbf{r}\,\mathrm{d}\mathbf{r}' + F^{B}[\rho_i(\mathbf{r})] \quad (21)$$

At equilibrium, the site density profile $\rho_i(\mathbf{r})$ minimizes the grand potentials of both the real and ideal-gas reference systems:

$$\frac{\delta\Omega[\rho_i(\mathbf{r})]}{\delta\rho_i(\mathbf{r})} = 0 \quad (22)$$

which leads to

$$\beta V_i^{\mathrm{ext}}(\mathbf{r}) - \beta V_{\mathrm{IG},i}^{\mathrm{ext}}(\mathbf{r}) = \sum_j \int c_{ij}^{(2)}(|\mathbf{r}-\mathbf{r}'|)\Delta\rho_j(\mathbf{r}')\,\mathrm{d}\mathbf{r}' - B_i(\mathbf{r}) \quad (23)$$

With the help of eqs 17 and 21, we substitute eq 23 back into eq 21 and derive the final expression of the solvation free energy:

$$\beta F[\rho_i(\mathrm{r})] = -\Delta N + \frac{1}{2} \sum_{i,j} \iint c_{ij}^{(2)}(|\mathbf{r}-\mathbf{r}'|) \times [\rho_i(\mathbf{r})\rho_j(\mathbf{r}) - \rho_i^{\mathrm{b}}\rho_j^{\mathrm{b}}]\,\mathrm{d}\mathbf{r}\,\mathrm{d}\mathbf{r}' + \beta F^{\mathrm{B}}[\rho_i(\mathbf{r})] - \sum_i \int \rho_i(\mathbf{r})B_i(\mathbf{r})\,\mathrm{d}\mathbf{r} \quad (24)$$

Equation 24 is another key result from this work. In using this equation, we first calculate the site−site DCFs from MD simulations for the bulk solvent. Then, the site density profiles of the solvent molecules near different solutes are calculated iteratively from eq 7 with the bridge functional from eq 14, and finally we compute the solvation free energies from eq 24.

III. COMPUTATIONAL METHODS AND NUMERICAL PROCEDURES

We use the standard OPLS-AA force field for the molecular analogs of amino-acid side chains. The same force field was also used in molecular simulations[13,19] that will be compared with the theoretical results. The site−site interaction $v_{ij}(|\mathbf{r}-\mathbf{r}_j|)$ between the solute and water molecules is expressed as the Lennard-Jones (LJ) potential plus the Coulomb potential. The LJ force field parameters follow the conventional Lorentz combining rule. All calculations are performed in three-dimensional cubic grid space with the mass center of the solute molecule fixed at the origin. The box length is set as 32 Å to 40 Å, depending on the solute size. The resolution of local density profiles is set at 0.25 Å in all directions. Larger box sizes and higher grid resolutions have been tested, but we found that the maximum deviation of the solvation free energy is no more than 0.1 kcal/mol.

To improve computational efficiency, we separate the site−site DCFs into short- and long-range contributions

$$c_{ij}^{(2)}(r) = c_{ij}^{\mathrm{SR}}(r) + c_{ij}^{\mathrm{LR}}(r) \quad (25)$$

The long-range component $c_{ij}^{\mathrm{LR}}(r)$ is expressed as the asymptotic relation[51]

$$c_{ij}^{\mathrm{LR}}(r) = -\zeta\beta\frac{q_i q_j}{4\pi\varepsilon_0 r} \quad (26)$$

As shown in Appendix B, the convolution between the long-range part DCFs and the local density can be expressed as

$$k_\mathrm{B}T \sum_j \int \Delta\rho_j(\mathbf{r}')c_{ij}^{\mathrm{LR}}(|\mathbf{r}-\mathbf{r}'|)\,\mathrm{d}\mathbf{r}' = q_i^{\mathrm{eff}}\Psi(\mathbf{r}) \quad (27)$$

where $q_i^{\mathrm{eff}} = q_i\sqrt{\zeta}$ and $\Psi(\mathbf{r})$ is an effective intrinsic electrostatic potential that satisfies

$$\nabla^2\Psi(\mathbf{r}) = -\sum_i \frac{q_i^{\mathrm{eff}}\rho_i(\mathbf{r})}{\varepsilon_0} \quad (28)$$

Equation 28 can be solved with the finite element method. Here, we use the Intel Poisson solver package.

The Fast Fourier Transform (FFT) method is used to calculate the convolution between the short-range DCFs and the local density

$$\int f_1(\mathbf{r}')f_2(\mathbf{r}-\mathbf{r}')\,\mathrm{d}\mathbf{r}' = \mathcal{F}^{-1}\{\mathcal{F}[f_1(\mathbf{r})]\mathcal{F}[f_2(\mathbf{r})]\} \quad (29)$$

where $\mathcal{F}$ and $\mathcal{F}^{-1}$ represent the forward and the backward FFT, respectively. The FFT method is also used in the MFMT calculations. The detailed equations are presented in Appendix

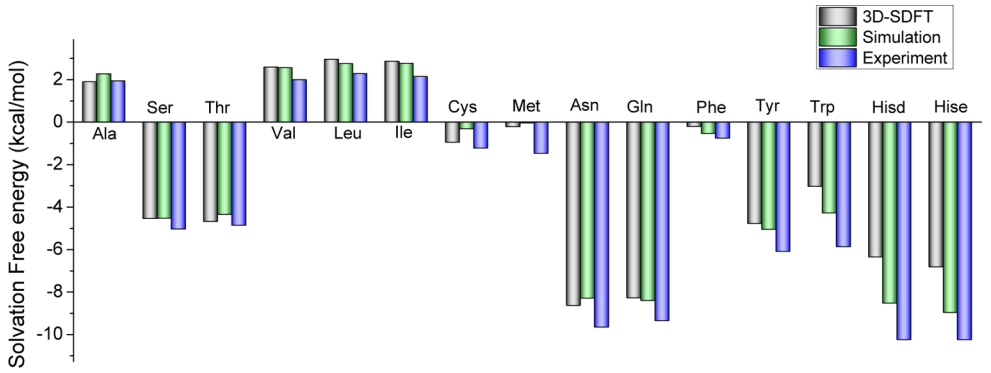

Figure 1. Solvation free energies of the amino-acid side chains calculated from the SPC/E model compared with simulation[13] and experimental[5] data (unit: kcal/mol).

C. In this work, all Fourier transforms were calculated from the FFTW module. For the integrals appearing in $S_\alpha(\mathbf{r})$, we used the Gauss-Legendre numerical integration method.

The computational cost of the 3D-SDFT calculations is mainly affiliated with the Picard iteration for solving the 3D density profiles of atomic sites. To ensure convergence and numerical efficiency, we adopted the following computational procedure during the iteration. The maximum deviation at the nth step is defined as

$$\Delta_n = \max\{|\rho_i^{(n)}(\mathbf{r}) - \rho_{i,\mathrm{new}}^{(n)}(\mathbf{r})|/\rho_i^{\mathrm{bulk}}\} \tag{30}$$

where $\rho_{i,\mathrm{new}}^{(n)}(\mathbf{r})$ represents the newly updated density profile from eqs 7 and 8 based on $\rho_i^{(n)}(\mathbf{r})$ generated at the nth step. The density profile for the $(n+1)$th step is obtained from

$$\rho_i^{(n+1)} = w^{(n)}\rho_i^{(n)}(\mathbf{r}) + (1 - w^{(n)})\rho_{i,\mathrm{new}}^{(n)}(\mathbf{r}) \tag{31}$$

The weighted parameter, $w^{(n)}$, varies along the iteration

$$\begin{cases} w^{(n)} = 0.9w^{(n-1)} + 0.095 & \Delta_n < \Delta_{n-1} \\ w^{(n)} = 0.1w^{(n-1)} + 0.9 & \Delta_n > \Delta_{n-1} \end{cases} \tag{32}$$

The initial guesses for $\rho_i(\mathbf{r})$ and w are irrelevant to the final result. The convergence tolerance is set as $\Delta = 10^{-3}$. To speed up the calculation, we do not update the local density at all grid points rigorously. Specifically, we update the local density $\rho(x_i, y_i, z_k)$ with the formula introduced above for all grid points if $(x_i^2 + y_j^2 + z_k^2)^{1/2} < 6$ Å; $i = 2m$, $j = 2n$, and $k = 2l$ if 6 Å $< (x_i^2 + y_j^2 + z_k^2)^{1/2} < 8$ Å; $i = 4m$, $j = 4n$, and $k = 4l$ if 8 Å $< (x_i^2 + y_j^2 + z_k^2)^{1/2} <$ 10 Å; $i = 8m$, $j = 8n$, and $k = 8l$ if 10 Å $< (x_i^2 + y_j^2 + z_k^2)^{1/2} < 12$ Å; and $i = 16m$, $j = 16n$, and $k = 16l$ if 12 Å $< (x_i^2 + y_j^2 + z_k^2)^{1/2}$. Here, m, n, and l are integer numbers. In all cases, the numerical values at the remaining grid points are calculated by linear interpolation.

IV. NUMERICAL RESULTS AND DISCUSSION

We have implemented the 3D-SDFT both with and without the bridge functional. By omitting the bridge terms in eq 7 and eq 9, the 3D-SDFT is essentially the same as the CMS theory, but because of the difference in calculation of the DCFs, we refer to the simplified version as SDFT-HNC. By contrast, the one with the reference HS bridge terms is called SDFT-HNCB. Both versions were used to calculate the solvation free energies of 15 molecular analogs of amino acid side chains in water at 298 K. In these calculations, the water molecules are represented by three popular classical models, SPC/E, SPC, and TIP3P, and the water-solute interactions are specified by the OPLS-AA force field. The theoretical predictions are compared with two sets of experimental results and two sets of simulation data. The discrepancy between different sets of simulation and experimental data provides a measure of the numerical performance.

Figure 1 shows the solvation free energies of amino acid side chains in SPC/E water from SDFT-HNCB, direct MD simulations, and experiments.[13] For more extensive comparisons, Table 1 presents the corresponding numerical values, along with the results from SDFT-HNC, alternative simulation data,[13,49] and experimental measurements.[5,47] For all solutes except Trp and His (Hisd and Hise) side-chain analogues, the predictions from the SDFT-HNCB agree well with both the simulation and experimental data. The higher deviations for tryptophan and histidine are probably related to the inaccuracy of the LJ potential for heteroring molecules. Overall, the average deviation for the SDFT-HNCB predictions of the SFEs is about 1.22 kcal/mol in comparison with experiments and 0.59 kcal/mol in comparison with simulation. Because there are comparable discrepancies between simulation results and

Table 1. Solvation Free Energies of Side Chains Calculated from Different Versions of 3D-SDFT and from Molecular Dynamic Simulations Using the SPC/E for Water and OPLS-AA Force Field for Side Chain Analogues in Comparison with Experimental Data (unit: kcal/mol)

	experiment		simulation		3D-SDFT	
side chain analogues	Wolfenden[a]	Cabani[b]	Pande[c]	Vegt[d]	HNC	HNCB
Ala	1.94	2.00	2.27	2.25	7.06	1.90
Ser	−5.06	−5.11	−4.55	−4.57	0.45	−4.56
Thr	−4.88	−5.01	−4.37	−4.57	3.11	−4.70
Val	1.99	1.96	2.56	2.53	13.8	2.59
Leu	2.28	2.32	2.75	2.65	17.1	2.96
Ile	2.15	2.08	2.76	2.63	17.08	2.87
Cys	−1.24	−1.24	−0.33	−0.31	6.63	−0.96
Met	−1.48		−0.05	−0.07	13.69	−0.23
Asn	−9.68	−9.71	−8.32	−8.46	−0.13	−8.66
Gln	−9.38		−8.42	−7.67	2.71	−8.30
Phe	−0.76	−0.89	−0.54	−0.65	15.2	−0.22
Tyr	−6.11	−6.14	−5.07	−5.19	11.85	−4.79
Trp	−5.88		−4.30	−4.57	17.39	−3.04
Hisd	−10.27		−8.55		5.31	−6.37
Hise	−10.27		−8.99		5.5	−6.84

[a]Ref 5. [b]Ref 45. [c]Ref 14. [d]Ref 47.

dx.doi.org/10.1021/ct3010936 | J. Chem. Theory Comput. 2013, 9, 1896−1908

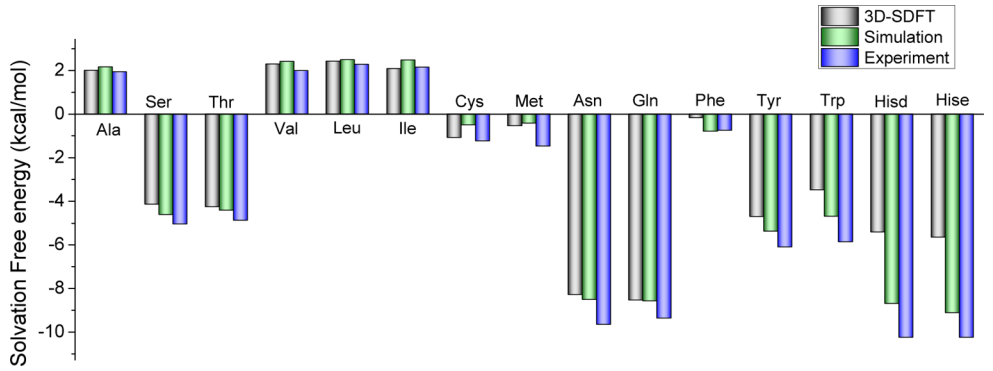

Figure 2. Solvation free energies of the amino-acid side chains calculated from the SPC model compared with simulation[13] and experimental[5] data (unit: kcal/mol).

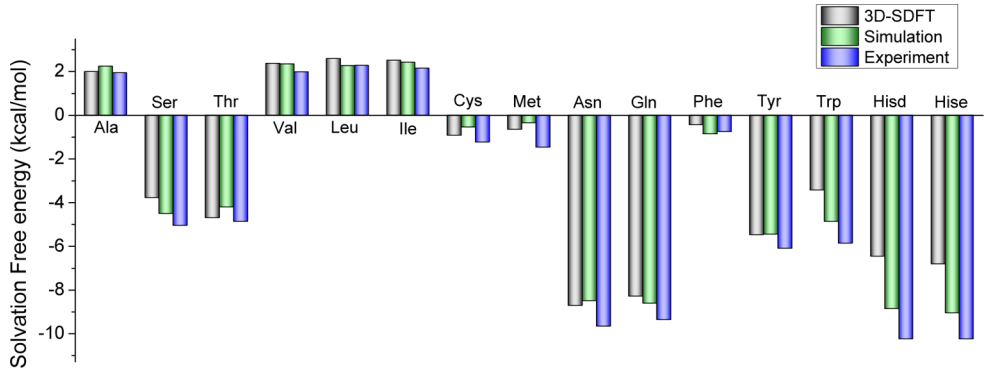

Figure 3. Solvation free energies of the amino-acid side chains calculated from the TIP3P model compared with simulation[13] and experimental[5] data (unit: kcal/mol).

Table 2. Solvation Free Energies of Side Chains Predicted from Theory and Simulation Using the SPC Water Model in Comparison with Experimental Data (unit: kcal/mol)

	experiment		simulation		3D-SDFT	
side chain analogues	Wolfenden[a]	Cabani[b]	Pande[c]	Tieleman[d]	HNC	HNCB
Ala	1.94	2.00	2.17	2.22	7.36	2.00
Ser	−5.06	−5.11	−4.62	−4.42	1.15	−4.15
Thr	−4.88	−5.01	−4.43	−4.61	4.91	−4.26
Val	1.99	1.96	2.41	2.70	16.09	2.30
Leu	2.28	2.32	2.50	3.01	20.22	2.43
Ile	2.15	2.08	2.48	2.84	20.14	2.08
Cys	−1.24	−1.24	−0.50	−0.26	7.80	−1.09
Met	−1.48		−0.42	−1.22	17.26	−0.54
Asn	−9.68	−9.71	−8.53	−8.20	3.39	−8.30
Gln	−9.38		−8.59	−7.36	5.19	−8.56
Phe	−0.76	−0.89	−0.79	−0.33	21.77	−0.18
Tyr	−6.11	−6.14	−5.39	−4.35	17.83	−4.71
Trp	−5.88		−4.70	−3.61	23.78	−3.49
Hisd	−10.27		−8.71	−6.50	9.86	−5.43
Hise	−10.27		−9.14	−6.50	10.49	−5.66

[a]Ref 5. [b]Ref 45. [c]Ref 14. [d]Ref 48.

experimental data, we consider the performance of the 3D-SDFT very satisfactory.

Table 1 shows that the SDFT-HNCB preforms significantly better than SDFT-HNC for molecular solvation in SPC/E water. In general, SDFT-HNC greatly overestimates the solvation free energies of all solutes by more than 10 kcal/mol. The comparison between the two versions of 3D-SDFT reveals that the bridge functional is an essential contribution to the solvation free-energy calculation. To a certain degree, the good agreement with the simulation results further validates that the universality ansatz for the bridge functional (eq 15) provides a good approximation for predicting the excluded volume effects on the solvation free energy. The importance of the bridge functional has also been found in 3D-RISM theory[4,25] as well as in density functional calculation of ion solvation.[38,59]

Figures 2 and 3 show similar comparisons but for SPC and TIP3P water models, respectively. The numerical values from different approaches are listed in Tables 2 and 3. Overall, the

dx.doi.org/10.1021/ct3010936 | J. Chem. Theory Comput. 2013, 9, 1896−1908

Table 3. Solvation Free Energies of Side Chains from Theory and Simulation of TIP3P Water in Comparison with Experimental Data (unit: kcal/mol)

	experiment		simulation		3D-SDFT	
side chain analogue	Wolfenden[a]	Cabani[b]	Pande[c]	Vegt[d]	HNC	HNCB
Ala	1.94	2.00	2.24	2.20	6.43	2.00
Ser	−5.06	−5.11	−4.51	−4.54	0.80	−3.79
Thr	−4.88	−5.01	−4.22	−4.49	3.09	−4.71
Val	1.99	1.96	2.34	2.39	11.96	2.38
Leu	2.28	2.32	2.27	2.53	14.6	2.59
Ile	2.15	2.08	2.43	2.46	14.51	2.52
Cys	−1.24	−1.24	−0.55	−0.48	5.57	−0.93
Met	−1.48		−0.35	−0.41	11.11	−0.66
Asn	−9.68	−9.71	−8.51	−8.65	−0.48	−8.73
Gln	−9.38		−8.63	−7.84	2.54	−8.31
Phe	−0.76	−0.89	−0.86	−0.91	12.95	−0.45
Tyr	−6.11	−6.14	−5.46	−5.71	7.86	−5.48
Trp	−5.88		−4.88	−4.92	13.04	−3.43
Hisd	−10.27		−8.88		3.18	−6.47
Hise	−10.27		−9.08		3.30	−6.83

[a]Ref 5. [b]Ref 45. [c]Ref 14. [d]Ref 47.

numerical performance of 3D-SDFT is the same as those for the SPC/E water: most theoretical results agree well with experiments and simulations except slightly larger deviations for the histidine side-chain analogues. As for the SPC/E model, SDFT-HNC is not very accurate for all cases. Inclusion of the bridge contribution dramatically improves the numerical performance. In comparison with the experimental data, the average deviation of the theoretical predictions for the SPC model is 1.27 kcal/mol, and for TIP3P it is 1.09 kcal/mol. In comparison with simulations, the corresponding deviations are 0.76 kcal/mol for SPC and 0.64 kcal/mol for TIP3P. We should indicate that the TIP3P model shows the best results comparing to experiments because the OPLS force field is originally parametrized with the TIP family of water models.

While the hybrid methods rely on the simulation results as an input,[8,9,38] the 3D-SDFT predicts the 3D density profiles of the surrounding solvent molecules in a self-consistent manner. For example, Figure 4 shows the density profile of the oxygen site surrounding the Leu side-chain analog dissolved in SPC/E water at the $x = 0$ plane. Figure 4a presents the density profile from the MD simulation carried with Moldy[60] over 100 000 configurations, and Figure 4b and c present those from 3D-SDFT/HNC and 3D-SDFT/HNCB, respectively. The 3D density profile of the solvent is related to the position and orientation of the dissolved solute. In all three cases, the Leu side-chain analog is fixed at the center of the computational box with the atomic coordinates specified in the Supporting Information.

In general, both HNC and HNCB versions of 3D-SDFT catch the outline of the solvation structure from the MD simulation. Apparently, 3D-SDFT/HNC significantly overestimates the first peak, which is similar to the case in MDFT/HRFA.[29] Inclusion of the reference HS bridge reduces the first peak and makes the theoretical result closer to the simulation. Such change reveals that the bridge function behaves as an effective repulsive potential. Nevertheless, the discrepancy of 3D-SDFT/HNCB from the simulation result is clearly visible. Although the first peak is noticeably improved comparing to the HNC prediction, HNCB underestimates the simulation value. The same situation occurs for the second peak in the solvent distributions. Such

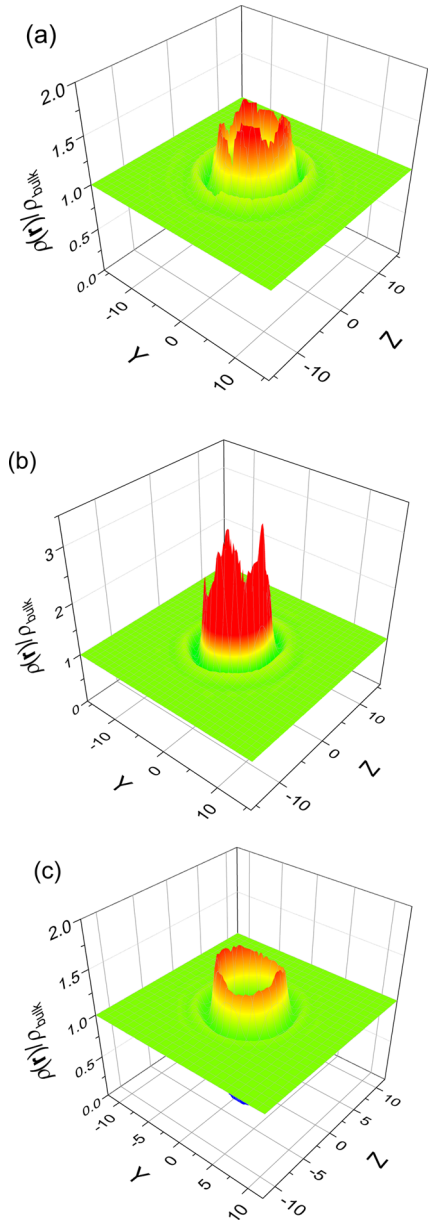

Figure 4. Reduced density profile of the oxygen site of SPC/E water near the Leu side-chain analog at the $x = 0$ plane from (a) MD simulation, (b) DFT-HNC prediction, and (c) DFT-HNCB prediction (length unit: angstrom). The Leu side chain analog is fixed at the box center with identical coordination in three cases (see Supporting Information).

overcorrection of solvent structure over HNC has been similarly identified for the 3D-RISM/HNCB theory.[61] Most likely the overcorrection arises from the approximations of the solute−solvent bridge functions. In the present work, we approximate the solute−oxygen bridge with that from an inhomogeneous reference of a HS system while neglecting the solute−hydrogen bridge term. Such treatment fails to capture the charge-dipole multibody correlation as discussed in the framework of 1D integral-equation theories.[62,63] Since the tetrahedral structure of water can be successfully reproduced through either proper two-body long-range interactions or three-body short-range interaction,[64] in this spirit, inclusion of an additional solute−hydrogen bridge term or a three-body empirical bridge term[29]

dx.doi.org/10.1021/ct3010936 | J. Chem. Theory Comput. 2013, 9, 1896−1908

may be promising toward further improvement for simultaneous predictions of both the solvation structure and free energy.

Whereas the numerical procedure of the 3D-SDFT calculation is probably more complicated than typical molecular simulation methods, a major advantage of the DFT-based methods is the minimal computational cost. For example, the computational time of our 3D-SDFT method for calculating the solvation free energy can be measured in terms of a desktop computer with a single node of a 3 GHz CPU. For a 32 Å × 32 Å × 32 Å box, it takes less than 15 min for the solvation free energy calculation; for a 40 Å × 40 Å × 40 Å box, the free-energy calculation can be finished within a few hours.

V. CONCLUSIONS

In this work, we have presented a novel three-dimensional site density functional theory (3D-SDFT) and demonstrated its numerical performance by studying the solvation free energies of 15 amino-acid side chain analogs in water. We have selected these systems not only because of their apparent biological significance but also because of the ready availability of high-quality simulation and experimental data for comparison. Unlike the angular description of the solvent molecules that requires the computation of high-dimensional density and correlation functions, the site DFT developed here incorporates the site−site direct correlation functions from MD simulation and Rosenfeld's universality *ansatz* for the bridge functional. Within the framework of the 3D-SDFT, we can readily calculate the solvation structure in terms of the site density profiles of the solvent molecules as well as the solvation free energy.

We have demonstrated the numerical performance of the 3D-SDFT by comparing with simulation and experimental data for the solvation free energies of 15 amino acid side chains in water. In the theoretical calculations, the water molecules are represented by SPC/E, SPC, and TIP3P models, and all side chains are characterized by the OPLS-AA force field. For all water models, the bridge functional is approximated by that of an inhomogeneous hard-sphere reference system with the density profile identical to the density distribution of the oxygen atoms. For each water model, the effective hard-sphere diameter is determined by matching the theoretical value to the experimental hydration free energy of methane, the simplest side chain analogue. The bridge functional of the hydrogen site is omitted in the current calculation. For all cases, the effective hard-sphere diameter is close to the realistic diameter of a water molecule.

In implementation of the 3D-SDFT, the density profiles of oxygen and hydrogen sites are solved iteratively on a 3D grid of variable resolution. With the input of oxygen and hydrogen density profiles, the solvation free energies of 15 amino acid side chains have been calculated and compared with the corresponding simulation and experimental data. While molecular simulation of the solvation free energy has been notoriously difficult, for all systems considered in this work, the DFT calculation takes only several tens of minutes using a single computer process. Besides, the 3D-SDFT predictions are in excellent agreement with both simulations and experiments results. For the TIP3P model, the average deviations are about 1.09 kcal/mol in comparison with experimental measurements and about 0.64 kcal/mol in comparison with simulation values.

We have also compared the numerical performance of the 3D-SDFT with and without the bridge functional contributions. While the computational costs for these two versions of SDFT are similar, we find that the bridge functional, which originates from the molecular excluded volume effects, makes an important contribution to the solvation free energies of all side chains. In particular, the SDFT-HNC method drastically overestimates the solvation free energies of hydrophobic solutes.

The computational efficiency and numerical accuracy make the 3D-SDFT useful for studying the solvation properties of large solutes, albeit under that circumstance, we must account for the internal flexibility of the solute properly. Application of 3D-DFT for the solvation of flexible molecules will be addressed in future work.

APPENDIX A. SOLVATION FREE ENERGY IN AN IDEAL REFERENCE SYSTEM

In this appendix, we derive the equation used to calculate the solvation free energy in an ideal-gas reference system. Consider an open system of ideal gas molecules under an external potential. The grand partition function reads

$$\begin{aligned}\Xi &= \sum_{N=0}^{\infty} \frac{1}{N!(\prod_\alpha \Lambda_\alpha)^N \nu^N} \left[\int \mathrm{d}\mathbf{R} \exp\{-\beta \sum_\alpha^M \psi_\alpha(\mathbf{r}) - \beta W(\mathbf{R})\}\right]^N \\ &= \exp\left\{\frac{1}{\nu \prod_\alpha \Lambda_\alpha} \int \mathrm{d}\mathbf{R} \exp\{-\beta \sum_\alpha^M \psi_\alpha(\mathbf{r}) - \beta W(\mathbf{R})\}\right\} \end{aligned} \tag{A1}$$

Here, Λ_α denotes the thermal wavelength of atom α, and M is the total number of atoms within each molecule, ν is the symmetry number, $W(\mathbf{R})$ is the bonding potential with $\mathbf{R} = (\mathbf{r}_1, ...\mathbf{r}_\alpha, ..., \mathbf{r}_M)$ being the molecular coordinate, and $\psi_\alpha(\mathbf{r})$ is defined by the difference between atom (site) chemical potential μ_α and the external potential $V_\alpha^{\mathrm{ext}}(\mathbf{r})$

$$\psi_\alpha(\mathbf{r}) = V_\alpha^{\mathrm{ext}}(\mathbf{r}) - \mu_\alpha \tag{A2}$$

The grand potential follows

$$\begin{aligned}\Omega &= -k_\mathrm{B}T \ln \Xi \\ &= -k_\mathrm{B}T \frac{1}{\nu \prod_\alpha \Lambda_\alpha} \int \mathrm{d}\mathbf{R} \exp\{-\beta \sum_\alpha^M \psi_\alpha(\mathbf{r}) - \beta W(\mathbf{R})\}\end{aligned} \tag{A3}$$

A functional derivative of the grand potential gives the one-body site density

$$\begin{aligned}\rho_\alpha(\mathbf{r}) &= -\frac{\delta\Omega}{\delta\psi_\alpha(\mathbf{r})} \\ &= \frac{1}{\nu \prod_\alpha \Lambda_\alpha} \int \mathrm{d}\mathbf{R} \exp\{\beta \sum_\alpha^M \psi(\mathbf{r}_\alpha) - \beta W(\mathbf{R})\}\delta(\mathbf{r} - \mathbf{r}_\alpha)\end{aligned} \tag{A4}$$

A comparison of eq A3 to eq A4 yields

$$\Omega = -k_\mathrm{B}T \int \rho_\alpha(\mathbf{r})\, \mathrm{d}\mathbf{r} \tag{A5}$$

Because the grand potential should be immaterial to dummy variable α, the integral can be replaced by

dx.doi.org/10.1021/ct3010936 | J. Chem. Theory Comput. 2013, 9, 1896−1908

$$\Omega = -\frac{k_B T}{M} \sum_{\alpha}^{M} \int \rho_\alpha(\mathbf{r})\, d\mathbf{r} \tag{A6}$$

In the above derivation, the density profile is not specified; therefore eq A6 is valid for both bulk and inhomogeneous systems.

The solvation free energy of a rigid solute is the difference between the grand potential of the solvated system and that of the initial bulk system

$$\begin{aligned} \Delta\Omega &= \Omega[\rho_\alpha(\mathbf{r})] - \Omega[\rho^b] \\ &= -\frac{k_B T}{M} \sum_{\alpha}^{M} \int (\rho_\alpha(\mathbf{r}) - \rho^b)\, d\mathbf{r} \\ &\equiv -\Delta N k_B T \end{aligned} \tag{A7}$$

Equation A7 can be applied to calculate the solvation free energy of any rigid solute immersed in an ideal molecular gas.

APPENDIX B. POISSON EQUATION FOR CALCULATING THE CONVOLUTION OF THE LONG-RANGE DIRECT CORRELATION FUNCTION WITH THE LOCAL DENSITY

In this appendix, we prove that the Poisson equation can be used to evaluate the convolution integral for the long-range contribution of the direct correlation functions. For convenience, here we consider only a simple spherical solute dissolved in water. But extension of the derivation for a more complicated solute is straightforward.

As discussed in the main text, the direct correlation function can be decomposed in to a short-range part (SR) and a long-rang part (LR)

$$c_{ij}^{SR}(r) = c_{ij}(r) - c_{ij}^{LR}(r) \tag{B1}$$

with the LR part follows an expression similar to that from the mean-spherical approximation (MSA)

$$c_{ij}^{SR}(r) = -\zeta\beta U_{ij}^{qq}(r) \tag{B2}$$

Here, $U_{ij}^{qq}(r) = q_i q_j/(4\pi\varepsilon_0 r)$ is the bare Coulomb potential between site i and site j. $\beta = 1/(k_B T)$ is the inverse temperature, and ζ is a state-dependent parameter arising from the intramolecular correlations but independent of specific site pairs.

For a solute dissolved in this solvent system, the mean electric potential $\Psi(\mathbf{r})$ at position $\mathbf{r}$ follows the Poisson equation

$$\nabla^2\Psi(\mathbf{r}) = -\frac{\rho_{ext}(\mathbf{r}) + \sum_i z_i e \rho_i(\mathbf{r})}{\varepsilon_0} \tag{B3}$$

where $\rho_i(\mathbf{r})$ is the local density of solvent site i with charge valence z_i, and $\rho_{ext}(\mathbf{r})$ is the charge density distribution of the solute. For a rigid solute with a point charge, $\rho_{ext}(\mathbf{r})$ can be expressed in terms of the Dirac delta function

$$\rho_{ext}(\mathbf{r}) = \sum_s q_s \delta(\mathbf{r} - \mathbf{r}_s) \tag{B4}$$

where q_s and $\mathbf{r}_s$ are the charge and position of the solute sites, respectively. In writing eq B4, we use a coordinate system with the solute charge placed at the origin.

A Fourier transform on both sides of eq B3 yields

$$-k^2\mathcal{F}[\Psi(\mathbf{r})] = -\mathcal{F}\left[\frac{\rho_{ext}(\mathbf{r})}{\varepsilon_0}\right] - \mathcal{F}\left[\frac{\sum_i z_i e \rho_i(\mathbf{r})}{\varepsilon_0}\right] \tag{B5}$$

Formally, the mean electrostatic potential can be obtained by the inverse Fourier transform

$$\Psi(\mathbf{r}) = \mathcal{F}^{-1}\left\{\frac{1}{k^2}\mathcal{F}\left[\frac{\rho_{ext}(\mathbf{r})}{\varepsilon_0}\right]\right\} + \mathcal{F}^{-1}\left\{\frac{1}{k^2}\mathcal{F}\left[\frac{\sum_i z_i e \rho_i(\mathbf{r})}{\varepsilon_0}\right]\right\} \tag{B6}$$

In eqs B5 and B6, $\mathcal{F}$ and $\mathcal{F}^{-1}$ represent the forward and the backward Fourier transforms, respectively.

Using eq B4, we can evaluate the first term on the right-hand-side of eq B6 analytically

$$\mathcal{F}^{-1}\left\{\frac{1}{k^2}\mathcal{F}\left[\frac{\rho_{ext}(\mathbf{r})}{\varepsilon_0}\right]\right\} = \sum_s \frac{q_s}{4\pi\varepsilon_0|\mathbf{r} - \mathbf{r}_s|} \equiv \Psi^{ext}(\mathbf{r}) \tag{B7}$$

where $\Psi^{ext}(\mathbf{r})$ is defined as the external electrostatic potential due to the solute, and together with the Lennard-Jones potential between solute and solvent site i, it recovers the total external potential exerting on site i, viz.,

$$V_i^{ext}(r) = V_{LJ-i}^{ext}(r) + z_i e \Psi^{ext}(r) \tag{B8}$$

Denote the second term on right-hand side of eq B6 as

$$\Psi^{int}(\mathbf{r}) = \mathcal{F}^{-1}\left\{\frac{1}{k^2}\mathcal{F}\left[\frac{\sum_i z_i e \rho_i(\mathbf{r})}{\varepsilon_0}\right]\right\} \tag{B9}$$

Thus, we have $\Psi(\mathbf{r}) = \Psi^{ext}(\mathbf{r}) + \Psi^{int}(\mathbf{r})$. That is, the mean electric potential $\Psi(\mathbf{r})$ has two contributions, and one is from the external electronic potential, while the other, $\Psi^{int}(r)$, is the intrinsic part due to the solvent charge. Multiply $-\zeta\beta z_i$ on both sides of eq B9 and use eq B2

$$\begin{aligned} -\zeta\beta z_i e \Psi^{int}(\mathbf{r}) &= -\mathcal{F}^{-1}\left\{\frac{4\pi}{k^2}\mathcal{F}\left[\frac{\sum_j \zeta\beta z_i z_j e^2}{4\pi\varepsilon_0}\rho_j(\mathbf{r})\right]\right\} \\ &= \sum_j \mathcal{F}^{-1}\{\mathcal{F}[-\zeta\beta U_{ij}^{qq}(\mathbf{r})]\mathcal{F}[\rho_j(\mathbf{r})]\} \\ &= \sum_j \mathcal{F}^{-1}\{\mathcal{F}[c_{ij}^{LR}(\mathbf{r})]\mathcal{F}[\rho_j(\mathbf{r})]\} \\ &= \sum_j \int c_{ij}^{LR}(|\mathbf{r} - \mathbf{r}'|)\rho_j(\mathbf{r}')\, d\mathbf{r}' \\ &= \sum_j \int c_{ij}^{LR}(|\mathbf{r} - \mathbf{r}'|)\Delta\rho_j(\mathbf{r}')\, d\mathbf{r}' \\ &\quad + \rho_j^b \sum_j \int c_{ij}^{LR}(|\mathbf{r} - \mathbf{r}'|)\, d\mathbf{r}' \\ &= \sum_j \int c_{ij}^{LR}(|\mathbf{r} - \mathbf{r}'|)\Delta\rho_j(\mathbf{r}')\, d\mathbf{r}' \end{aligned} \tag{B10}$$

To arrive at the final equality, we have applied the overall charge neutrality of the solvent molecules, viz.

dx.doi.org/10.1021/ct3010936 | J. Chem. Theory Comput. 2013, 9, 1896−1908

$$\sum_j \int c_{ij}^{\mathrm{LR}}(|\mathbf{r}-\mathbf{r}'|)\,\mathrm{d}\mathbf{r}' = \sum_j \int -\frac{\zeta\beta z_i z_j e^2}{4\pi\varepsilon_0|\mathbf{r}-\mathbf{r}'|}\,\mathrm{d}\mathbf{r}' = -\zeta\beta z_i \int \frac{\sum_j z_j e^2}{4\pi\varepsilon_0|\mathbf{r}-\mathbf{r}'|}\,\mathrm{d}\mathbf{r}' = 0 \tag{B11}$$

Thus, the convolution of the site−site DCF with the local density can be written as

$$\sum_j \int \Delta\rho_j(\mathbf{r}')c_{ij}^{(2)}(|\mathbf{r}-\mathbf{r}'|)\,\mathrm{d}\mathbf{r}' = \sum_j \int c_{ij}^{\mathrm{SR}}(|\mathbf{r}-\mathbf{r}'|)\Delta\rho_j(\mathbf{r}')\,\mathrm{d}\mathbf{r}' - \beta z_i e\zeta\Psi^{\mathrm{int}}(\mathbf{r}) \tag{B12}$$

Now rescale the site charge $z_i^{\mathrm{eff}} \equiv z_i\sqrt{\zeta}$ and the intrinsic electric potential $\Psi^{\mathrm{eff}}(\mathbf{r}) \equiv \sqrt{\zeta}\Psi^{\mathrm{int}}(\mathbf{r})$. Eq B10 becomes

$$\sum_j \int \Delta\rho_j(\mathbf{r}')c_{ij}^{\mathrm{LR}}(|\mathbf{r}-\mathbf{r}'|)\,\mathrm{d}\mathbf{r}' = \beta z_i^{\mathrm{eff}} e\Psi^{\mathrm{eff}}(\mathbf{r}) \tag{B13}$$

The effective intrinsic electric potential satisfies the Poisson equation

$$\nabla^2\Psi^{\mathrm{eff}}(\mathbf{r}) = -\sum_i \frac{z_i^{\mathrm{eff}} e\rho_i(\mathbf{r})}{\varepsilon_0} \tag{B14}$$

Equation B14 can be solved from any standard Poisson solver.

APPENDIX C. MODIFIED FUNDAMENTAL MEASURE THEORY IMPLEMENTED WITH THE FAST FOURIER TRANSFORM

Real-space calculations are efficient for implementation of the modified fundamental measure theory (MFMT) for systems with one-dimensional inhomogeneity but not for systems with higher degrees of inhomogeneity. In this work, we use the Fast Fourier Transform (FFT) to speed up the calculations. Here, we present the main equations used in our calculation.

In MFMT, excess Helmholtz free energy $F_{\mathrm{HS}}^{\mathrm{ex}}$ is related to the excess Helmholtz energy density $\Phi(\mathbf{r})$

$$F_{\mathrm{ex}} = k_{\mathrm{B}}T\int \mathrm{d}\mathbf{r}\,\Phi(\mathbf{r}) \tag{C1}$$

Here, k_{B} is the Boltzmann constant and T is the system temperature. The excess Helmholtz energy density $\Phi(\mathbf{r})$ is a function of seven weighted densities

$$\chi(\mathbf{r}) = -n_0\ln(1-n_3) + \frac{n_1n_2 - \mathbf{n}_{V1}\cdot\mathbf{n}_{V2}}{1-n_3} + \frac{n_3 + (1-n_3)^2\ln(1-n_3)}{36\pi n_3^2(1-n_3)^2}(n_2^3 - 3n_2\mathbf{n}_{V2}\cdot\mathbf{n}_{V2}) \tag{C2}$$

Here, n_α (α = 0, 1, 2, 3, $V1$, and $V2$) are weighted density (note that $\mathbf{n}_{V1}$ and $\mathbf{n}_{V2}$ are vectors), and it can be calculated using the Fourier transform and convolution theorem

$$n_\alpha(\mathbf{r}) = \int \rho(\mathbf{r})\omega_\alpha(\mathbf{r}-\mathbf{r}')\,\mathrm{d}\mathbf{r}' = \mathcal{F}^{-1}[\mathcal{F}(\rho)\mathcal{F}(\omega_\alpha)] = \mathcal{F}^{-1}[\rho(\mathbf{k})\omega_\alpha(\mathbf{k})] \tag{C3}$$

In the above equation, $\rho(\mathbf{r})$ and $\rho(\mathbf{k})$ are the local density in the real space and the Fourier space, respectively. $\omega_\alpha(\mathbf{k})$ are weight functions, and their expressions in the Fourier space are

$$\omega_0(\mathbf{k}) = \omega_0(k) = \begin{cases} \dfrac{\sin(Rk)}{Rk} & k \neq 0 \\ 1 & k = 0 \end{cases} \tag{C4}$$

$$\omega_1(\mathbf{k}) = \omega_1(k) = \begin{cases} \dfrac{\sin(Rk)}{k} & k \neq 0 \\ R & k = 0 \end{cases} \tag{C5}$$

$$\omega_2(\mathbf{k}) = \omega_2(k) = \begin{cases} \dfrac{4\pi R\,\sin(Rk)}{k} & k \neq 0 \\ 4\pi R^2 & k = 0 \end{cases} \tag{C6}$$

$$\omega_3(\mathbf{k}) = \omega_3(k) = \begin{cases} \dfrac{4\pi}{k^3}[\sin(Rk) - Rk\cos(Rk)] & k \neq 0 \\ 4\pi R^3/3 & k = 0 \end{cases} \tag{C7}$$

$$\omega_{V1}(\mathbf{k}) = \frac{1}{4\pi R}\omega_{V2}(\mathbf{k}) \tag{C8}$$

$$\omega_{V2}(\mathbf{k}) = \begin{cases} \dfrac{-4\pi i}{k^3}[\sin(Rk) - Rk\cos(Rk)]\mathbf{k} & k \neq 0 \\ 0 & k = 0 \end{cases} \tag{C9}$$

where R represents the hard-sphere radius.

With the product of $\rho(\mathbf{k})$ and $\omega_\alpha(\mathbf{k})$ in the Fourier space and followed with a reverse Fourier transform, we can get $n_\alpha(\mathbf{r})$, which is an essential quantity in calculating the overall excess Helmholtz free energy from eq C2 and eq C1 and in calculating the local excess chemical potential via

$$\beta\mu_i^{\mathrm{ex}}(\mathbf{r}) = \frac{\delta\beta F_{\mathrm{ex}}}{\delta\rho_i(\mathbf{r})} = \sum_\alpha \int \mathrm{d}\mathbf{r}'\,\upsilon_\alpha\omega_\alpha(\mathbf{r}'-\mathbf{r}) \tag{C10}$$

In the above equation, the summation applies to the weighted densities of the fundamental measure theory, $\beta = 1/k_{\mathrm{B}}T$ and $\upsilon_\alpha = \partial\Phi(\mathbf{r})/\partial n_\alpha$. From $n_\alpha(\mathbf{r})$, we can readily calculate

$$\upsilon_0 = -\ln(1-n_3) \tag{C11}$$

$$\upsilon_1 = \frac{n_2}{1-n_3} \tag{C12}$$

$$\upsilon_2 = \frac{n_1}{1-n_3} + \left[\frac{\ln(1-n_3)}{n_3} + \frac{1}{(1-n_3)^2}\right]\frac{n_2^2 - \mathbf{n}_{V2}^2}{12\pi n_3} \tag{C13}$$

dx.doi.org/10.1021/ct3010936 | J. Chem. Theory Comput. 2013, 9, 1896−1908

$$\upsilon_3 = \frac{n_0}{1-n_3} + \frac{n_1 n_2 - \mathbf{n}_{V1}\cdot\mathbf{n}_{V2}}{(1-n_3)^2} - \frac{n_2^3 - 3n_2\mathbf{n}_{V2}^2}{36\pi n_3^2} \times \left[\frac{2 - 5n_3 + n_3^2}{(1-n_3)^3} + \frac{2\ln(1-n_3)}{n_3}\right] \quad \text{(C14)}$$

$$\upsilon_{v1} = -\frac{\mathbf{n}_{V2}}{1-n_3} \quad \text{(C15)}$$

$$\upsilon_{v2} = -\frac{\mathbf{n}_{v1}}{1-n_3}\left[\frac{\ln(1-n_3)}{n_3} + \frac{1}{(1-n_3)^2}\right]\frac{n_2\mathbf{n}_{v2}}{6\pi n_3} \quad \text{(C16)}$$

Hereafter, we carry the forward Fourier transform to get $\upsilon_\alpha(\mathbf{k})$, and then followed by a reverse Fourier transform of the product $\upsilon_\alpha(\mathbf{k})\ \omega_\alpha(\mathbf{k})$, we finally get the reduced local excess chemical potential

$$\beta\mu_i^{\text{ex}}(\mathbf{r}) = \sum_\alpha \mathcal{F}^{-1}[\mathcal{F}(\upsilon_\alpha)\mathcal{F}(\omega_\alpha)] = \mathcal{F}^{-1}[\upsilon_\alpha(\mathbf{k})\omega_\alpha(\mathbf{k})] \quad \text{(C17)}$$

■ ASSOCIATED CONTENT

Ⓢ Supporting Information

The coordinates of the Leu side chain analog fixed at the center of the calculation box are provided. The coordinates are complementary to the atomic solvent density distributions presented in Figure 4. This material is available free of charge via the Internet at http://pubs.acs.org.

■ AUTHOR INFORMATION

Corresponding Author

*E-mail: szhao@ecust.edu.cn, jwu@engr.ucr.edu.

Notes

The authors declare no competing financial interest.

■ ACKNOWLEDGMENTS

For the financial support of this research, the authors are grateful to the U.S. Department of Energy (DE-FG02-06ER46296). S.Z. also acknowledges the support from the National Natural Science Foundation of China (No. 21206036) and the Fundamental Research Funds for the Centre Universities of China.

■ REFERENCES

(1) Hirata, F. *Molecular Theory of Solvation*: Kluwer Academic Publishers: Dordrecht, The Netherlands, 2003.
(2) Feig, M.; Onufriev, A.; Lee, M. S.; Im, W.; Case, D. A.; Brooks, C. L. *J. Comput. Chem.* **2004**, *25*, 265.
(3) Zou, X. Q.; Sun, Y. X.; Kuntz, I. D. *J. Am. Chem. Soc.* **1999**, *121*, 8033.
(4) Palmer, D. S.; Sergiievskyi, V. P.; Jensen, F.; Fedorov, M. V. *J. Chem. Phys.* **2010**, *133*, 044104.
(5) Wolfenden, R.; Andersson, L.; Cullis, P. M.; Southgate, C. C. B. *Biochemistry* **1981**, *20*, 849.
(6) Beglov, D.; Roux, B. *J. Chem. Phys.* **1996**, *104*, 8678.
(7) Chang, J.; Lenhoff, A. M.; Sandler, S. I. *J. Phys. Chem. B* **2007**, *111*, 2098.
(8) Freedman, H.; Le, L.; Tuszynski, J. A.; Truong, T. N. *J. Phys. Chem. B* **2008**, *112*, 2340.
(9) Freedman, H.; Truong, T. N. *Chem. Phys. Lett.* **2003**, *381*, 362.
(10) Paluch, A. S.; Shah, J. K.; Maginn, E. J. *J. Chem. Theory Comput.* **2011**, *7*, 1394.
(11) Jorgensen, W. L.; Ravimohan, C. *J. Chem. Phys.* **1985**, *83*, 3050.
(12) Duffy, E. M.; Jorgensen, W. L. *J. Am. Chem. Soc.* **2000**, *122*, 2878.
(13) Shirts, M. R.; Pande, V. S. *J. Chem. Phys.* **2005**, *122*, 134508.
(14) Jang, S.; Kim, E.; Pak, Y. *Proteins: Struct., Funct., Bioinf.* **2006**, *62*, 663.
(15) Born, M. *Z. Phys.* **1920**, *1*, 45.
(16) Marenich, A. V.; Olson, R. M.; Kelly, C. P.; Cramer, C. J.; Truhlar, D. G. *J. Chem. Theory Comput.* **2007**, *3*, 2011.
(17) Hansen, J. P.; McDonald, I. R. *Theory of Simple Liquids*, 3rd ed.; Academic Press: London, 2006.
(18) Gray, C. G.; Gubbins, K. E. *Theory of Molecular Fluids: Fundamentals*; Oxford University Press: New York, 1985; Vol *1*.
(19) Shirts, M. R.; Pitera, J. W.; Swope, W. C.; Pande, V. S. *J. Chem. Phys.* **2003**, *119*, 5740.
(20) Straatsma, T. P.; Berendsen, H. J. C. *J. Chem. Phys.* **1988**, *89*, 5876.
(21) Sandberg, L.; Edholm, O. *J. Chem. Phys.* **2002**, *116*, 2936.
(22) Jha, A. K.; Freed, K. F. *J. Chem. Phys.* **2008**, *128*, 034501.
(23) Cossi, M.; Scalmani, G.; Rega, N.; Barone, V. *J. Chem. Phys.* **2002**, *117*, 43.
(24) Cortis, C. M.; Rossky, P. J.; Friesner, R. A. *J. Chem. Phys.* **1997**, *107*, 6400.
(25) Du, Q. H.; Beglov, D.; Roux, B. *J. Phys. Chem. B* **2000**, *104*, 796.
(26) Gendre, L.; Ramirez, R.; Borgis, D. *Chem. Phys. Lett.* **2009**, *474*, 366.
(27) Ramirez, R.; Borgis, D. *J. Phys. Chem. B* **2005**, *109*, 6754.
(28) Ramirez, R.; Gebauer, R.; Mareschal, M.; Borgis, D. *Phys. Rev. E* **2002**, *66*, 031206.
(29) Zhao, S.; Ramirez, R.; Vuilleumier, R.; Borgis, D. *J. Chem. Phys.* **2011**, *134*, 194102.
(30) Ratkova, E. L.; Chuev, G. N.; Sergiievskyi, V. P.; Fedorov, M. V. *J. Phys. Chem. B* **2010**, *114*, 12068.
(31) Chandler, D. *Mol. Phys.* **1976**, *31*, 1213.
(32) Hirata, F.; Rossky, P. J. *Chem. Phys. Lett.* **1981**, *83*, 329.
(33) Kovalenko, A.; Hirata, F. *Chem. Phys. Lett.* **1998**, *290*, 237.
(34) Kovalenko, A.; Hirata, F.; Kinoshita, M. *J. Chem. Phys.* **2000**, *113*, 9830.
(35) Kovalenko, A.; Ten-No, S.; Hirata, F. *J. Comput. Chem.* **1999**, *20*, 928.
(36) Ladanyi, B. M.; Chandler, D. *J. Chem. Phys.* **1975**, *62*, 4308.
(37) Levesque, M.; Vuilleumier, R.; Borgis, D. *J. Chem. Phys.* **2012**, *137*, 034115.
(38) Zhao, S.; Jin, Z.; Wu, J. *J. Phys. Chem. B* **2011**, *115*, 15445.
(39) Borgis, D.; Levy, N.; Marchi, M. *J. Chem. Phys.* **2003**, *119*, 3516.
(40) Chandler, D.; McCoy, J. D.; Singer, S. J. *J. Chem. Phys.* **1986**, *85*, 5971.
(41) Seok, C.; Oxtoby, D. W. *J. Chem. Phys.* **1998**, *109*, 7982.
(42) Talanquer, V.; Oxtoby, D. W. *J. Chem. Phys.* **2003**, *118*, 872.
(43) Talanquer, V.; Oxtoby, D. W. *J. Chem. Phys.* **2001**, *114*, 2793.
(44) Reddy, G.; Lawrence, C. P.; Skinner, J. L.; Yethiraj, A. *J. Chem. Phys.* **2003**, *119*, 13012.
(45) Rosenfeld, Y. *Phys. Rev. Lett.* **1989**, *63*, 980.
(46) Lin, B.; Pettitt, B. M. *J. Comput. Chem.* **2011**, *32*, 878.
(47) Cabani, S.; Gianni, P.; Mollica, V.; Lepori, L. *J. Solution Chem.* **1981**, *10*, 563.
(48) Deng, Y.; Roux, B. *J. Phys. Chem. B* **2004**, *108*, 16567.
(49) Hess, B.; van der Vegt, N. F. A. *J. Phys. Chem. B* **2006**, *110*, 17616.
(50) Maccallum, J. L.; Tieleman, D. P. *J. Comput. Chem.* **2003**, *24*, 1930.
(51) Zhao, S.; Liu, Y.; Liu, H.; Wu, J. Submitted, 2013.
(52) Zhao, S.; Wu, J. *Mol. Phys.* **2011**, *109*, 2553.
(53) Rosenfeld, Y. *J. Chem. Phys.* **1993**, *98*, 8126.
(54) Rosenfeld, Y. *Phys. Rev. Lett.* **1994**, *72*, 3831.
(55) Yu, Y.-X.; Wu, J. *J. Chem. Phys.* **2002**, *117*, 10156.
(56) Roth, R.; Evans, R.; Lang, A.; Kahl, G. *J. Phys.: Condens. Matter* **2002**, *14*, 12063.
(57) Yu, Y. X.; You, F. Q.; Tang, Y. P.; Gao, G. H.; Li, Y. G. *J. Phys. Chem. B* **2006**, *110*, 334.
(58) Carnahan, N. F.; Starling, K. E. *J. Chem. Phys.* **1969**, *51*, 635.
(59) Kido, K.; Yokogawa, D.; Sato, H. *J. Chem. Phys.* **2012**, *137*, 024106.
(60) Refson, K. *Moldy User's Manual*; Department of Earth Sciences: Oxford, U. K., 2003.

(61) Perkyns, J. S.; Lynch, G. C.; Howard, J. J.; Pettitt, B. M. *J. Chem. Phys.* **2010**, *132*, 064106.
(62) Kusalik, P. G.; Patey, G. N. *Mol. Phys.* **1988**, *65*, 1105.
(63) Lombardero, M.; Martin, G.; Jorge, S.; Lado, F.; Lomba, E. *J. Chem. Phys.* **1999**, *110*, 1148.
(64) Molinero, V.; Moore, E. B. *J. Phys. Chem. B* **2009**, *113*, 4008.

NOTE ADDED AFTER ASAP PUBLICATION

This article was published ASAP on March 28, 2013. Changes have been made to equations 29, B5, B6, B9, B10, C3, and C17. The correct version was published on March 29, 2013.